SLAC-PUB-1814
September 1976
(T/E)

e^+e^- HADRON PRODUCTION AND JET STRUCTURE AT SPEAR*

GAIL G. HANSON

Stanford Linear Accelerator Center

Stanford University, Stanford, California 94305, U.S.A.

Abstract: Results on the total cross section for production of multihadronic events and inclusive distributions of the hadrons from e^+e^- annihilation in the center-of-mass energy range from 2.4 to 7.8 GeV are presented. Evidence for jet structure in the multihadronic events and the angular distributions of the hadrons and of the jet axis are reported. Inclusive distributions of hadrons in Feynman x, transverse momentum, and rapidity relative to the jet axis are presented.

(Talks given at the VIIth International Colloquium on Multiparticle Reactions, Tutzing/Munich, Germany, 21-25 June 1976, and the XVIIIth International Conference on High Energy Physics, Tbilisi, U.S.S.R., 15-21 July, 1976.)

*Work supported by the Energy Research and Development Administration.

I. INTRODUCTION

Measurements of hadron production by electron-positron annihilation for center-of-mass energies ($E_{c.m.}$) above 3 GeV have unearthed much exciting new physics. First, the total cross section for producing hadrons was found to be higher than expected.[1,2] Then the ψ and ψ' were discovered as sharp peaks in the total hadronic cross section.[3,4] The ψ' (and ψ) were found to decay to new narrow states.[5,6,7] Evidence for a heavy lepton was found in the form of events containing an electron and a muon with nothing else visible.[8] And finally, narrow states which may be the eagerly sought charmed mesons have been seen.[9,10]

In this talk I will discuss the properties of hadronic events produced in e^+e^- annihilation at SPEAR at energies away from the resonance regions. These events show evidence for jet structure, i.e., a limiting of transverse momentum relative to an axis. The jet axis has an angular distribution (measured at $E_{c.m.}$ = 7.4 GeV) which is consistent with a $1+\cos^2\theta$ distribution, the angular distribution for a pair of spin one-half particles. A quark-parton picture, with the addition of at least one new heavy quark, seems to be generally consistent with the data.

II. DETECTOR AND EVENT SELECTION

The data for this analysis were taken by the SLAC/LBL magnetic detector collaboration[11] at SPEAR. The SPEAR magnetic detector is shown schematically in Fig. 1. The detector consists of a 3-meter long, 3-meter diameter solenoid magnet with a 4 kG magnetic field parallel to the beam direction and wire spark chambers and scintillation counters for triggering and measuring events. The detector axis is centered on the beam direction at one of two interaction regions at SPEAR. Particles entering the detector from the interaction region can pass through, in order: a thin-walled vacuum chamber, inner cylindrical scintillation counters used in the trigger to reduce background from cosmic rays, inner

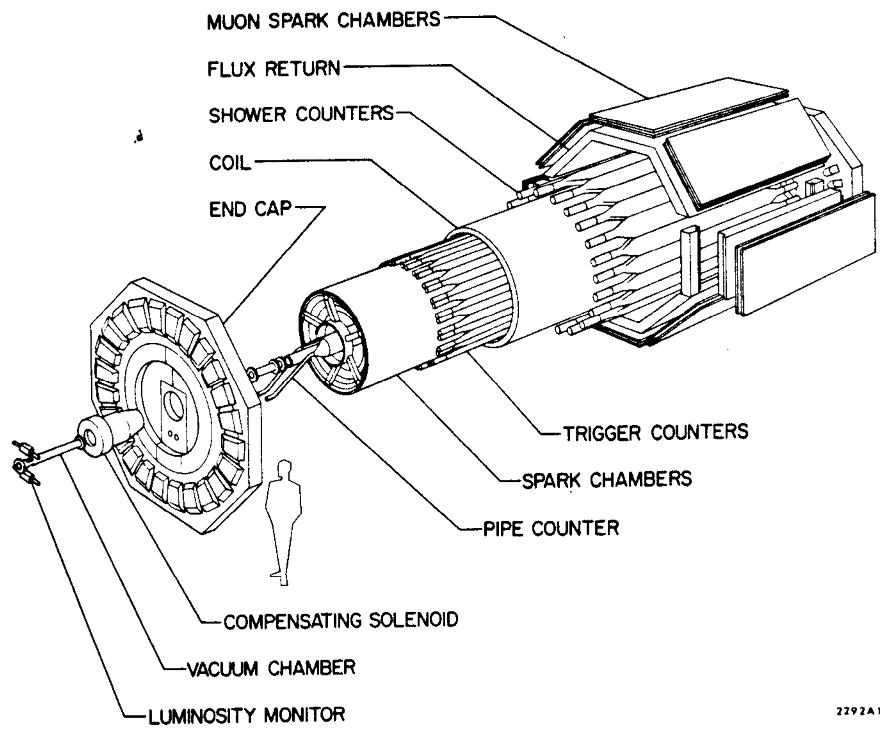

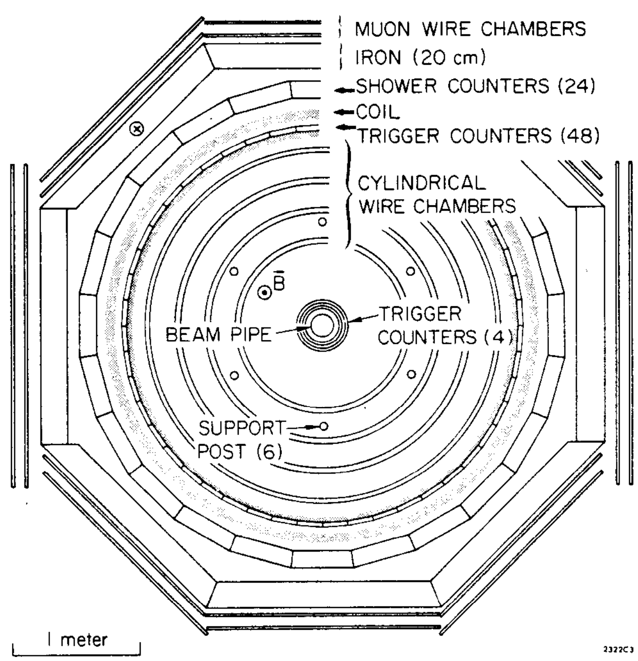

Fig. 1. Schematic diagrams of the SLAC/LBL magnetic detector.

multiwire proportional chambers, a system of cylindrical wire spark chambers, an array of trigger time-of-flight scintillation counters, the magnet coil, an array of lead-scintillator shower counters, the iron return yoke of the magnet, and finally wire spark chambers used for muon-hadron separation. The detector extends over 65% of 4π sr solid angle with full acceptance in azimuthal angle and acceptance in polar angle from 50° to 130°. The apparatus is triggered by two or more charged particles which produce signals in the inner scintillation counters and in at least two outer-trigger-counter-shower-counter combinations.

Events from the QED reactions

$$e^+e^- \rightarrow e^+e^- \quad \text{(Bhabha scattering)} \tag{1}$$

and

$$e^+e^- \rightarrow \mu^+\mu^- \tag{2}$$

were recorded simultaneously with the multihadronic events and provide a convenient normalization. Of those events originating from the interaction-region fiducial volume, those with two oppositely-charged prongs collinear within 10° were candidates for the QED reactions. Those with three or more prongs were classified as hadronic unless two prongs were collinear within 10° and had large shower-counter pulse height (consistent with electrons). Events in which there were two prongs acoplanar with the incident beam direction by at least 20° and in which both prongs had momenta greater than 300 MeV/c were also classified as hadronic. The detector and selection of events are described more fully in Refs. 2, 12, and 13.

III. GENERAL PROPERTIES OF MULTIHADRONIC EVENTS

In this section I will discuss the total cross section for multihadronic events, the mean charged particle multiplicity, and the inclusive momentum distributions of the hadrons. Jet structure and additional inclusive distributions of the hadrons will be discussed in Sections IV, V, and VI.

The total hadronic cross section was calculated from the total number of multihadronic events detected at each center-of-mass energy $E_{c.m.}$, corrected for losses due to geometric acceptance, triggering efficiency, cuts, and contamination from other sources. The cross section was normalized to the integrated luminosity obtained from Bhabha scattering events observed in the magnetic detector. A Monte Carlo simulation of the detector, described in more detail in Section IV, was used to estimate the losses due to geometric acceptance, triggering efficiency, and data analysis cuts. The model used for the production of hadronic events was generally invariant phase space; estimates of the model dependence are included in the systematic uncertainty. The Monte Carlo calculation resulted in a matrix of efficiencies for detecting a certain number of particles for each charged particle multiplicity in the produced state. The produced multiplicity distribution was then obtained as the maximum-likelihood solution to an overdetermined set of linear equations. The average detection efficiency was then obtained as simply the number of detected events divided by the number of produced events. The average detection efficiency varied from about 40% at the lowest energies to 60% at the highest energies. The increase in efficiency is due to the increase in multiplicity as the energy rises. The data were corrected for background from beam-gas scattering ($<8\%$ for $E_{c.m.}$ less than 5 GeV and $<5\%$ for $E_{c.m.}$ above 5 GeV) and from two-photon processes ($<2\%$). Radiative corrections have also been applied.

The total hadronic cross section σ_T as a function of $E_{c.m.}$ from 2.4 GeV to 7.8 GeV is shown in Fig.2(a). The error bars include statistical errors and our estimate of point-to-point systematic errors. The overall normalization uncertainty is $\pm 10\%$ and a further, smooth variation as large as 15% from the lowest energy to the highest energy could arise from systematic errors in the estimation of the average detection efficiency. The ψ and ψ' peaks are not shown. As $E_{c.m.}$ increases, σ_T falls except in the energy region around 4 GeV where at least two peaks in σ_T are seen. A discussion of the structure in the 4 GeV region is, unfortunately, not within the scope of this talk.

The ratio R of σ_T to the theoretical total cross section for production of muon pairs is presented in Fig. 2(b). In quark models for e^+e^- annihilation into hadrons

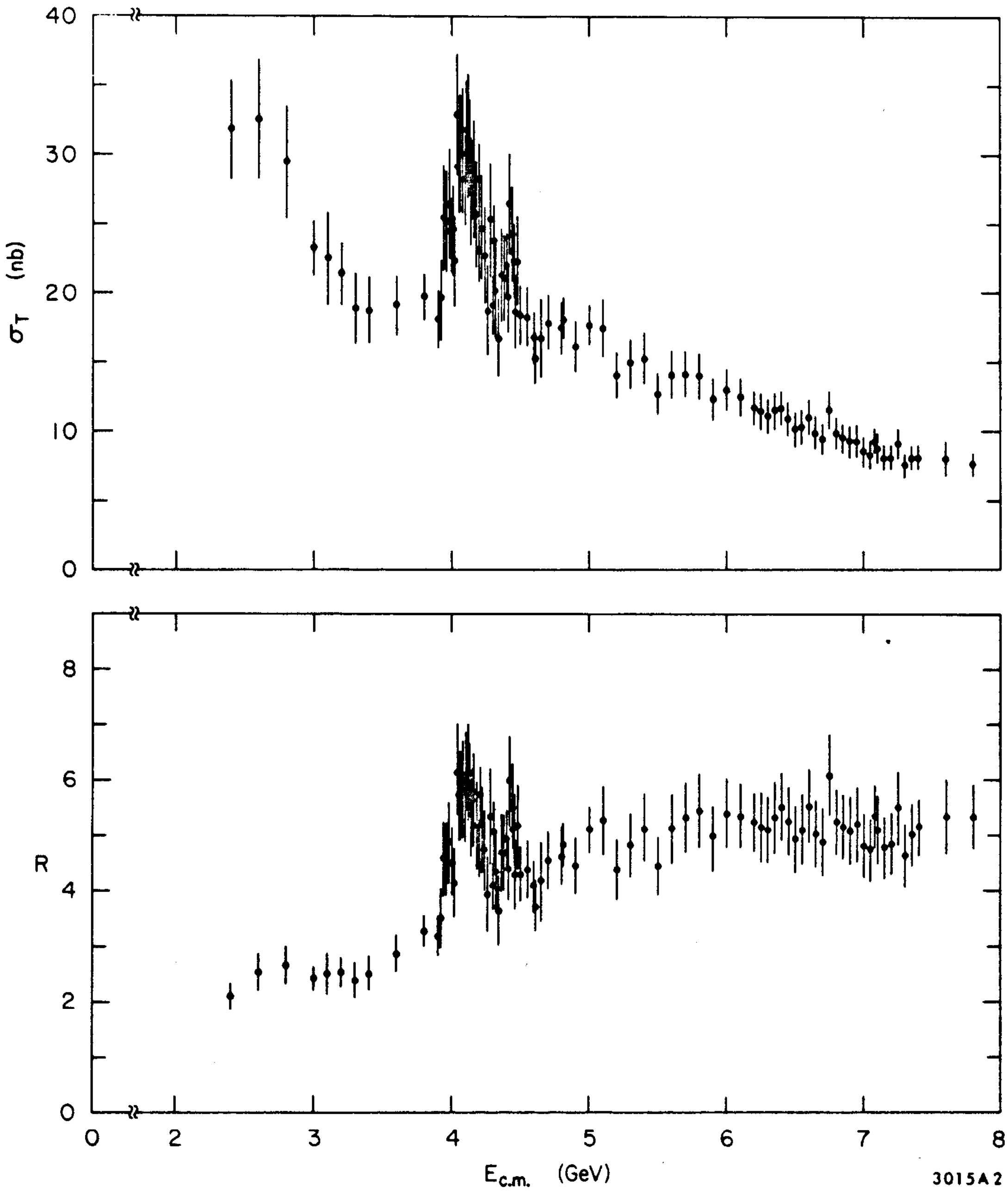

Fig. 2. (a) Total hadronic cross section σ_T vs. $E_{c.m.}$. (b) R vs. $E_{c.m.}$.

R is the sum of the squares of the charges of the expected spin-1/2 quarks. R is approximately constant at about 2.5 for $E_{c.m.}$ less than 3.5 GeV. As $E_{c.m.}$ increases R rises or perhaps goes through a step at the structure in the 4 GeV region. Above 4.8 GeV R is constant again at a value of about 5.5. The approximate doubling of R for energies above the 4 GeV structure suggests that the 4 GeV region may be a threshold region for production of new particles, or, in terms of the quark-theoretical interpretation, new quarks.

We have carried out a search for high-mass resonances which couple to e^+e^- by looking for bumps in R. Figure 3(a) shows the results of the search. The $E_{c.m.}$ ranges covered were 5.65 to 6.45 GeV and 6.97 to 7.45 GeV. The limiting energy resolution is the energy spread of SPEAR, which is ~1 MeV r.m.s. at $E_{c.m.}$ = 3 GeV and ~4 MeV r.m.s. at $E_{c.m.}$ = 6 GeV. We therefore scanned in 4 MeV steps. For the case of a resonance with an intrinsic width much narrower than the energy resolution, we are sensitive to the partial decay width to electron pairs Γ_e:

$$\int R(E)\, dE = \frac{3\pi}{2\alpha^2}(2J+1)\Gamma_e \quad ,$$

and for a wide resonance we are sensitive to the branching ratio to electron pairs B_e:

$$R(E_{c.m.}=M) = \frac{3}{\alpha^2}(2J+1)B_e \quad .$$

Figure 3(b) shows the 90% confidence upper limits for Γ_e or B_e for a J=1 resonance as a function of $E_{c.m.}$. For a narrow resonance in the 6 GeV region our upper limit is $\Gamma_e \lesssim 150$ eV and for a wide resonance $B_e \lesssim 10^{-5}$.

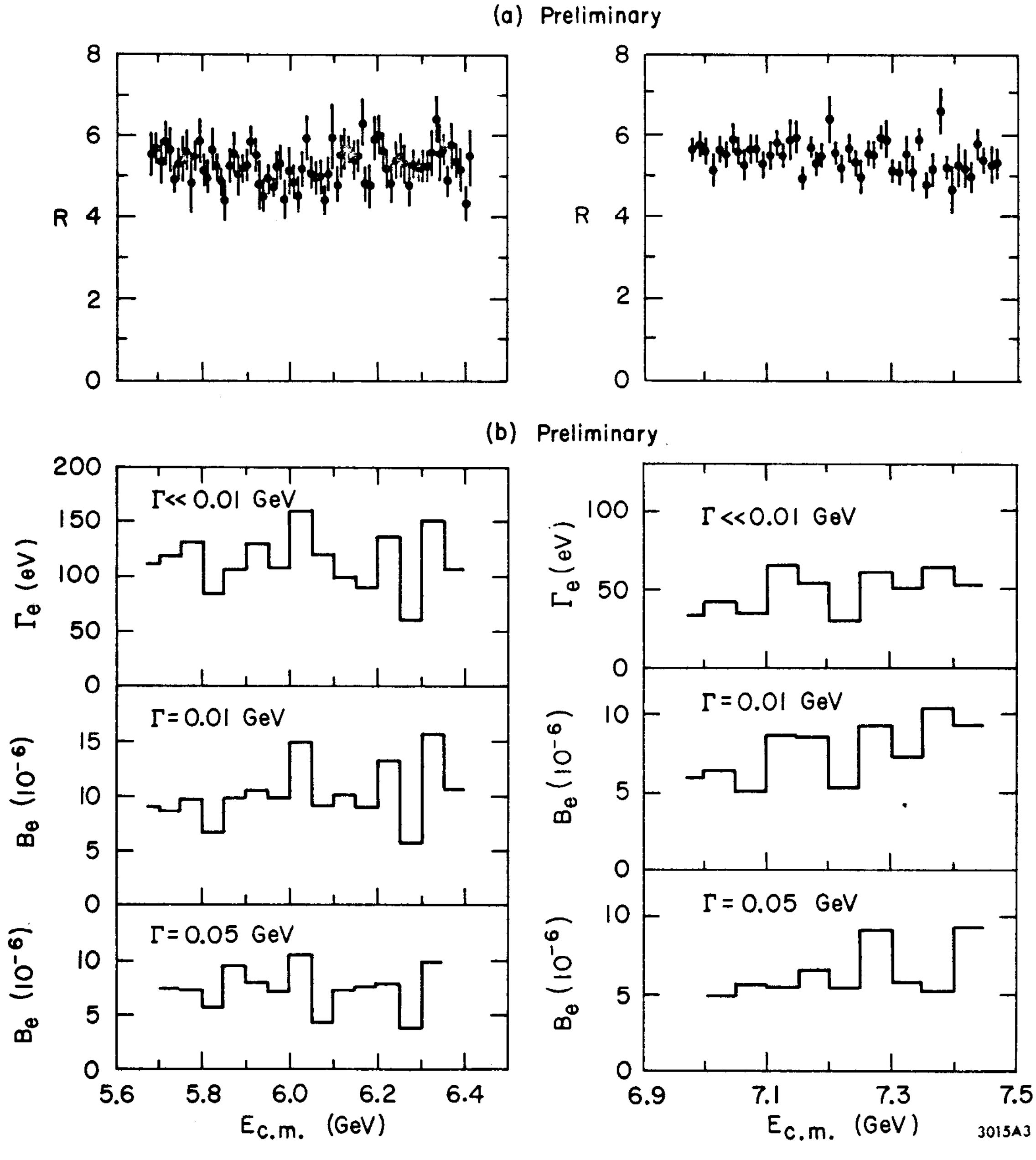

Fig. 3. (a) R vs. $E_{c.m.}$ in 10 MeV steps in the high energy region. (b) 90% confidence upper limits for Γ_e or B_e for a high-mass resonance decaying to e^+e^-.

The mean charged particle multiplicity $<n_{ch}>$ was obtained as part of the procedure described previously for determining the average detection efficiency and this is corrected for acceptance and trigger bias. Figure 4 shows $<n_{ch}>$

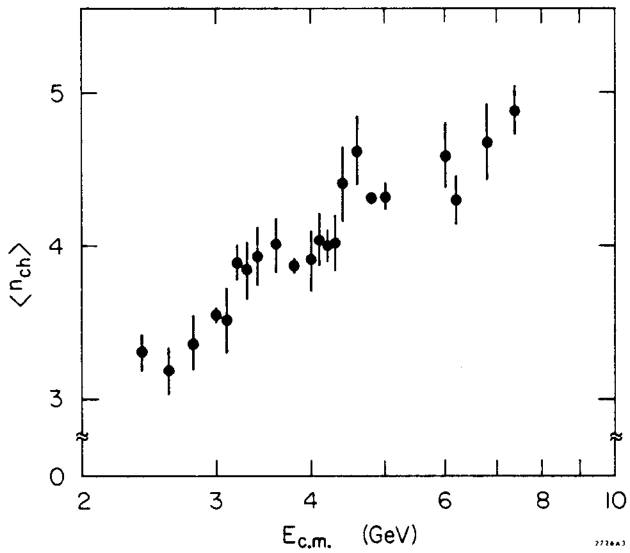

Fig. 4. Mean charged particle multiplicity $<n_{ch}>$ vs $E_{c.m.}$.

plotted versus the logarithm of $E_{c.m.}$. $<n_{ch}>$ rises from about 3 at the lowest energies to about 5 at the highest energies and is consistent with a logarithmic increase with energy.

At this point in the presentation of the multihadronic data only those multihadronic events with three or more detected charged particles will be used.[14] The two-prong events have so far been used only for the calculation of the total cross section and the mean charged particle multiplicity. The two-prong events are not used in further analyses because they are more subject to background contamination due to beam-gas interactions and two-photon processes.

The mean energy of observed tracks assuming pion masses, $<E_{track}>$, is shown as a function of $E_{c.m.}$ in Fig. 5. There is a hint of a break in the distribution near 4 GeV which may be a sign that appreciably more low momentum particles are being produced at energies above 4 GeV.

The mean fraction of energy in charged particles as a function of $E_{c.m.}$ is shown in Fig. 6. Pion masses are assumed for the particles. The data were

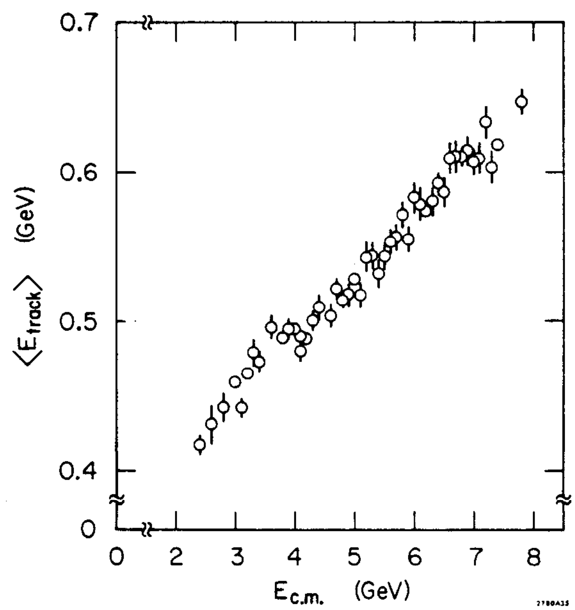

Fig. 5. Mean energy of observed tracks assuming pion masses vs. $E_{c.m.}$ for $\geq$ three prong events.

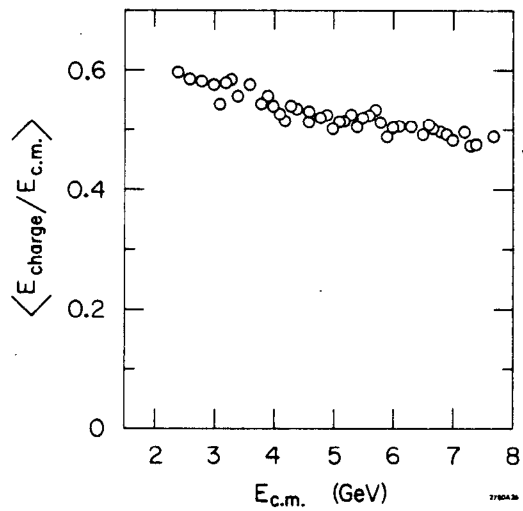

Fig. 6. Average fraction of energy appearing in charged particles vs. $E_{c.m.}$ for $\geq$ three prong events, assuming pion masses.

corrected for losses due to acceptance and trigger bias using the Monte Carlo simulation. The charged energy fraction decreases from 0.6 to 0.5 over the measured range of $E_{c.m.}$. This distribution presents the extension of the so-called "energy crisis" to the data above 5 GeV. If all the particles were pions, the charged energy fraction would be 2/3. Monte Carlo calculations show that the inclusion of kaons, etas, and nucleons should decrease the charged energy fraction by only a few percent. Neutrinos from heavy lepton decays should not contribute appreciably to the missing energy in this data sample (see Ref. 14).

Up to this point the data presented have been identical to those presented at the 1975 Lepton and Photon Symposium.[15] Since then a few minor problems with the high-energy data have been found. At energies above 7 GeV the photons from synchrotron radiation cause extra sparks in the spark chambers which our tracking algorithms sometimes used to form extra low-momentum tracks. The extra tracks led to more contamination from electromagnetic processes in the three-or-more-prong hadronic events which had the effect of adding prongs to the very low and high momentum ends of the inclusive momentum distributions. Tighter cuts were employed in the tracking algorithms and the data were reanalyzed.

Multiprong Bhabha scattering events (i.e., those with delta rays or converted photons) still posed a problem. The cut which removed events from the hadronic class if they had two prongs collinear within 10° and large shower counter pulse height was meant to remove these events. However, at high energies jet-like events were sometimes removed from the hadronic events by this cut. In addition, there were Bhabha scattering events in which the two electrons were acollinear which passed this cut. The total number of events involved was small (~ a few percent of the total) but they had a large effect on the high-momentum end of the momentum distributions. For these reasons the collinearity cut was changed to a cut which removed those events which had two oppositely-charged prongs coplanar within 5° with large shower counter pulse heights and momenta greater than 40% of the incident beam energy. Additional cuts were used on the three-, four-, and five-prong events to remove acoplanar multiprong Bhabha scattering events (e.g., an event with two electrons and a converted photon was considered to be electromagnetic). The cuts were checked by scanning the events affected in the 7.4 GeV data and were found to remove most Bhabha scattering events and very few hadronic events. The data presented in the remainder of this talk (except for Fig. 8) were analyzed using these new cuts.

Single particle inclusive momentum distributions have been studied for the large samples of data collected at $E_{c.m.} = 3.0$, 3.8, 4.8, 6.2, and 7.4 GeV. (Inclusive distributions for the 3.8 GeV data will not be presented here because they have not been reanalyzed with the radiative tail from the ψ' removed.) The raw momentum distributions for events in which three or more charged particles are detected are corrected for geometric acceptance and trigger bias using the Monte Carlo simulation. Radiative corrections have not been applied. In Fig. 7 the inclusive momentum distributions are presented in terms of the "experimental" scaling variable x

$$x = 2p/E_{c.m.} \quad , \tag{3}$$

where p is the particle momentum. The momentum is used instead of the energy because the particle identity is not measured for the entire momentum range. The quantity plotted is $s\,d\sigma/dx$ ($s = E^2_{c.m.}$) which is expected to scale at very high energies. The area under each curve is equal to $s\sigma_T \langle n_{ch}\rangle \propto R\langle n_{ch}\rangle$, so the area under the curve must increase as the energy increases. We see that these distributions roughly scale for $x \gtrsim 0.5$ for the entire energy range. The 3.0 GeV data seem to be systematically high for $x \geq 0.6$; however, systematic errors in the Monte Carlo corrections at the highest and lowest values of x could be as large as 20%. In addition, the detected two-prong events, which we do not use but correct for using the Monte Carlo simulation, form the largest fraction of the total number of events (25%) at 3.0 GeV. The 4.8, 6.2, and 7.4 GeV data scale rather well for $x \geq 0.2$.

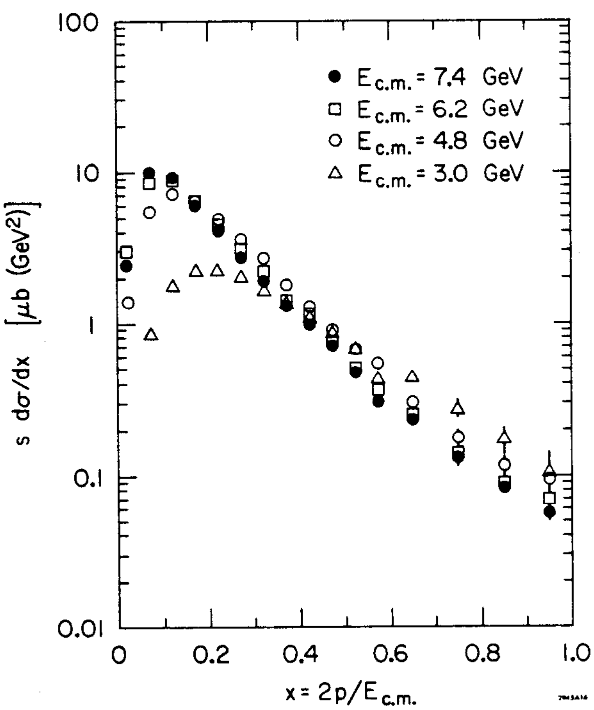

Fig. 7. $s\,d\sigma/dx$ vs. x for $E_{c.m.} = 3.0$, 4.8, 6.2, and 7.4 GeV.

We identify pions, kaons, and protons over a restricted momentum range using the time of flight measured by scintillation counters at 1.5 m from the beam line. The time-of-flight resolution is 0.4 nsec r.m.s. Kaons can be separated from pions for momenta less than 600 MeV/c, and protons can be separated from kaons and pions for momenta less than 1.1 GeV/c. Figure 8 shows the fractions of negative prongs which are kaons and antiprotons as a function of particle momentum for the large samples of data from 3.0 to 7.4 GeV and for the ψ. Negative prongs are used because the proton sample has a large contamination from beam-gas scattering. The kaon fraction increases from a few percent to about twenty percent as the momentum increases with very little dependence on $E_{c.m.}$, except that the fractions are consistently lower at the ψ. The antiproton fraction increases from zero to five or six percent, again with little dependence on $E_{c.m.}$.

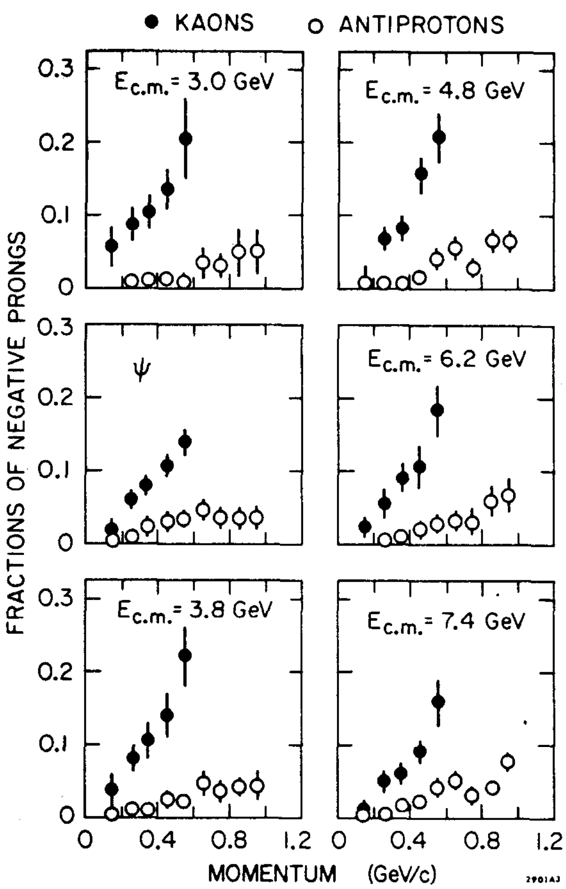

Fig. 8. Fractions of negative prongs which are kaons or antiprotons as a function of particle momentum for $E_{c.m.}$ = 3.0, 3.095 (= ψ), 3.8, 4.8, 6.2, and 7.4 GeV.

Of course, the momentum range over which we can separate particle types is quite limited. At $E_{c.m.}$ = 7.4 GeV, 600 MeV/c momentum corresponds to x = 0.16. In the range of momenta accessible to us phase space effects probably dominate. In order to test parton model predictions, for example, one needs to know the identity of the high-x particles.

IV. JET STRUCTURE

The motivation for searching for jet structure in hadron production by e^+e^- annihilation comes from quark-parton constituent models of elementary particles. In these models the e^+ and e^- annihilate to form a virtual photon which subsequently produces a quark-parton pair, each of which decays into hadrons, as shown in Fig. 9. At sufficiently high energy a two-jet structure is expected to arise due to the limited transverse momentum of the hadrons with respect to the original parton direction.[16-19] The spins of the constituents can, in principle, be determined from the angular distribution of the jets.

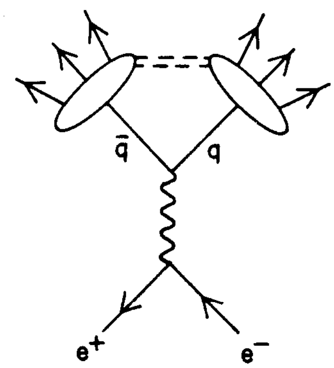

Fig. 9. Quark-parton model picture of production of hadrons in e^+e^- annihilation.

I will now describe the method used to search for jets. For each three or more prong hadronic event we find that direction which minimizes the sum of squares of transverse momenta. To do this, we diagonalize the tensor

$$T^{\alpha\beta} = \sum_i \left(\delta^{\alpha\beta}\vec{p}_i^{\,2} - p_i^\alpha p_i^\beta\right) , \tag{4}$$

where the summation is over all detected charged particles and α and β refer to the three spatial components of each particle momentum $\vec{p}_i$. $T^{\alpha\beta}$ is like a moment of inertia tensor, so what we are doing is finding principal moments in momentum space. We obtain the eigenvalues λ_1, λ_2, and λ_3 which are the sums of squares of transverse momenta with respect to the three eigenvector directions. The smallest eigenvalue λ_3 is the minimum sum of squares of transverse momenta, and the eigenvector direction associated with it is the reconstructed jet axis. This method of calculating the jet axis is not perfect. It is impossible to determine the jet axis exactly, even with perfect detection, unless one knows precisely which particle comes from which jet, in which case one could simply find the resultant momenta of two groups of particles. The method described here, which was suggested in Ref. 18, is the best approximation known to us.

In order to determine how jet-like an event is, we calculate a quantity which we call the sphericity S:

$$S = \frac{3\lambda_3}{\lambda_1+\lambda_2+\lambda_3} = \frac{3\left(\sum_i p_{\perp i}^2\right)_{min}}{2\sum_i \vec{p}_i^{\,2}} \quad . \tag{5}$$

S approaches 0 for events with limited transverse momentum (jet-like events) and approaches 1 for events with large multiplicity and isotropic phase space particle distributions.

Since the magnetic detector covered only part of the total solid angle and neutral particles were not detected, we needed to use a Monte Carlo simulation to determine how jet-like and isotropic hadronic events would differ in the detector. Events were generated according to either Lorentz-invariant phase space or a jet model in which phase space was modified by a matrix element squared of the form

$$M^2 = e^{-\left(\sum_i p_{\perp i}^2\right)/2b^2} \quad , \tag{6}$$

where $p_\perp$ is the momentum perpendicular to the jet axis. The jet axis angular distribution was of the form

$$\frac{d\sigma}{d\Omega} \propto 1 + \alpha \cos^2\theta \quad , \tag{7}$$

where θ is the polar angle relative to the e^+ beam. This angular distribution will be discussed in more detail when the measurement of the jet axis angular distribution is described. In both models only charged and neutral pions were produced, although some checks were performed using models which included kaons and etas. The total multiplicity was given by a Poisson distribution. The simulation included the geometric acceptance, trigger efficiency, momentum resolution, conversion probability for photons from π^o decay, and all other known characteristics of the detector.

We used the large samples of data collected at 3.0, 3.8, 4.8, 6.2, and 7.4 GeV. At each energy the total multiplicity and ratio of charged pions to neutral pions for both models were obtained by fitting to the observed charged particle mean momentum and mean multiplicity. The parameter b in the jet model was chosen by fitting to the observed mean $p_\perp$ with respect to the jet axis. The observed distribution of $p_\perp$ at 7.4 GeV is shown in Fig. 10 along with the predictions of the two models. The jet model reproduces the data rather well whereas phase space predicts too many particles at high $p_\perp$. The mean produced $p_\perp$ in the jet model was found to be in the range 325 to 360 MeV/c with no particular energy dependence. From hadron interaction data we would have expected the mean $p_\perp$ to be in the range 300 to 350 MeV/c.

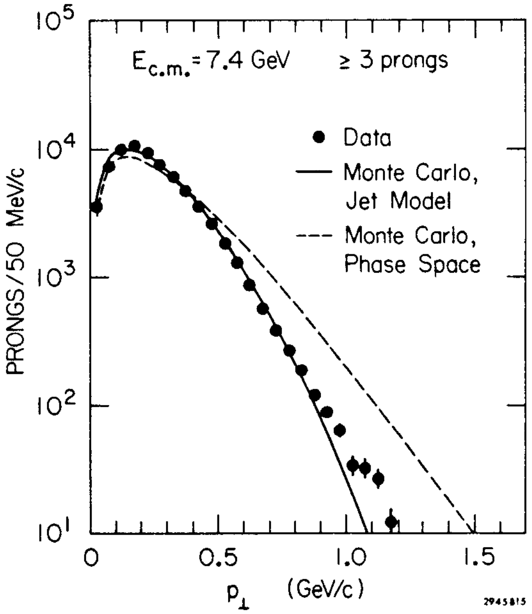

Fig. 10. Observed $p_\perp$ with respect to jet axis for 7.4 GeV data. The predicted distributions for the jet model (solid curve) and the phase-space model (dashed curve) are also shown.

The observed distributions of S can now be compared with the predictions of the two models. Figure 11 shows the observed S distributions for the lowest energy, 3.0 GeV, and for the two highest energies, 6.2 and 7.4 GeV. At 3.0 GeV the data agree with the predictions of either the jet model or the phase-space model (Fig. 11(a)). At this energy the limiting of transverse momentum to an average of 350 MeV/c has no effect on the phase-space particle distributions as manifested in the S distribution since the predictions of the two models are the same. At 6.2 and 7.4 GeV the S distributions are peaked toward low S favoring the jet model over the phase-space model (Figs. 11(b) and 11(c)).

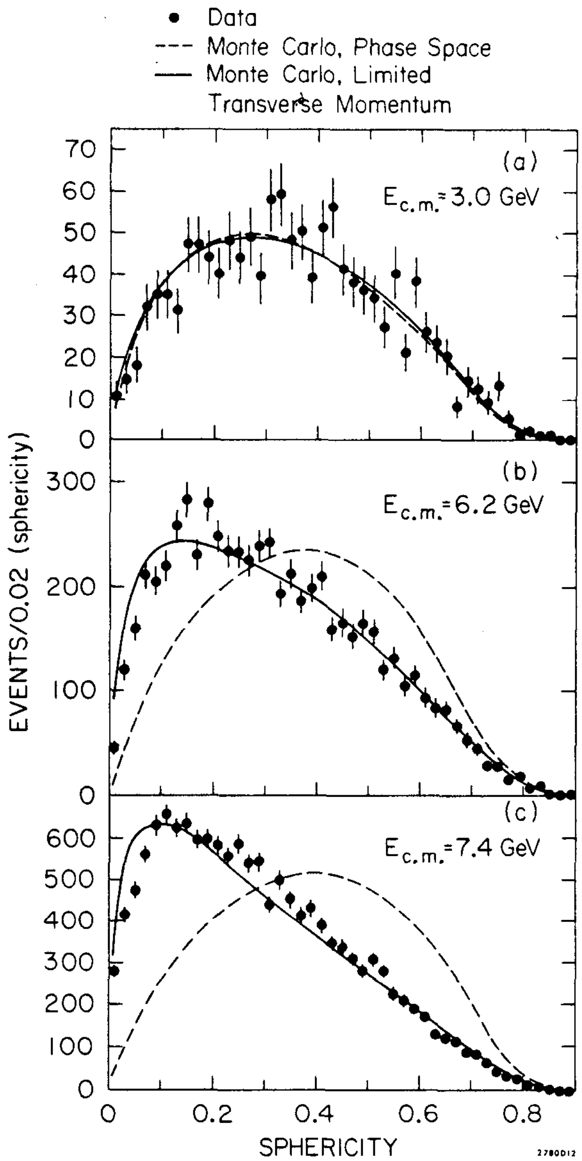

Fig. 11. Observed sphericity distributions for data, jet model (solid curves) and phase-space model (dashed curves) for (a) $E_{c.m.} = 3.0$ GeV, (b) $E_{c.m.} = 6.2$ GeV, and (c) $E_{c.m.} = 7.4$ GeV.

Figure 12 shows the S distribution at 7.4 GeV compared with the predictions of both a jet model and a phase-space model in which kaons and etas are produced along with pions. Etas and π^0's were produced with equal probability before phase-space effects, and kaon fractions were fitted to agree with the data for particle momenta less than 600 MeV/c (see Fig. 8). The conclusion is unchanged—the data favor the jet model.

The difference between the jet model and phase-space model predictions for the sphericity as a function of energy can be seen quantitatively in Fig. 13, which shows the observed mean S versus $E_{c.m.}$. The phase-space model predicts that the mean S should increase as $E_{c.m.}$ increases whereas the jet model predicts that the mean S should decrease. The data clearly show a decreasing mean S with increasing $E_{c.m.}$, in agreement with the jet model.

The agreement of the observed sphericity distributions with the jet model as opposed to the phase-space model is evidence for jet structure in e^+e^- hadron production. Differences in the exact shape of the S distributions between the data and the jet model can be caused by, among other things, differences in the exact

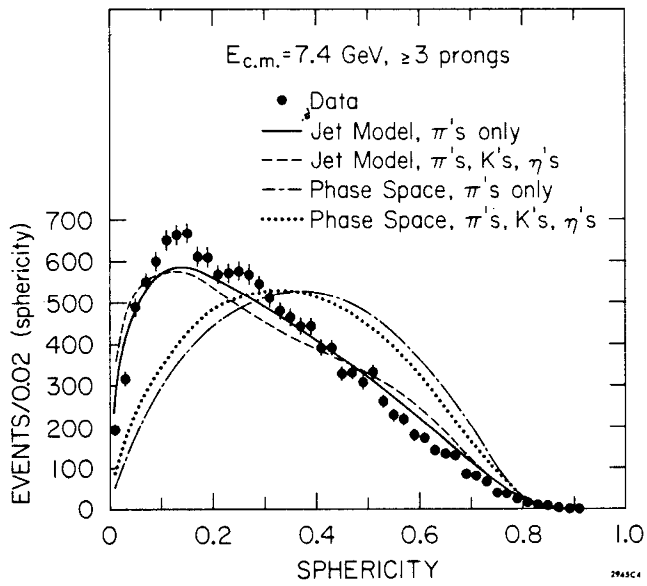

Fig. 12. Observed sphericity distribution at $E_{c.m.}$ = 7.4 GeV compared with prediction for jet model with pions only (solid curve), jet model with pions, kaons, and etas (dashed curve), phase-space model with pions only (dashed-dotted curve), and phase-space model with pions, kaons, and etas (dotted curve).

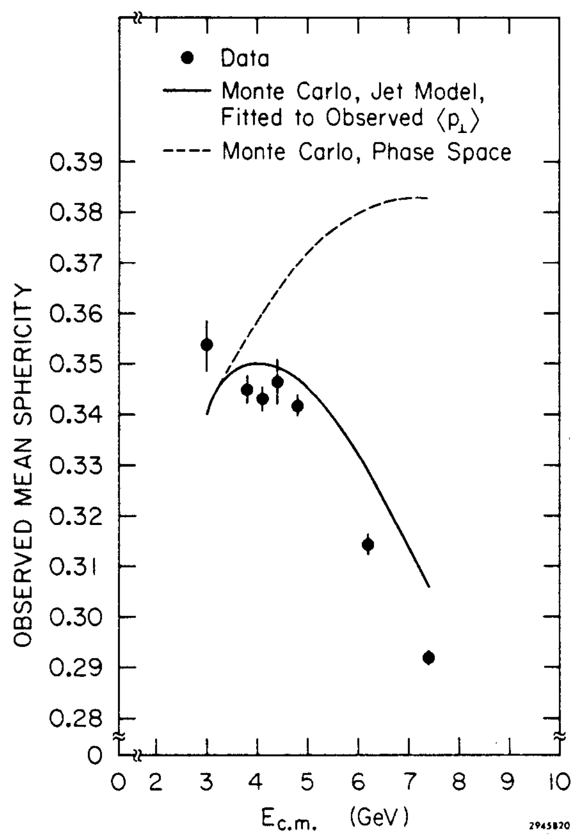

Fig. 13. Observed mean sphericity vs. $E_{c.m.}$ for data, jet model (solid curve), and phase-space model (dashed curve).

shape of the multiplicity distributions. The evidence for jet structure is corroborated by the distributions of the cosine of the angle between any pair of particles, shown in Fig. 14. At 6.2 and 7.4 GeV the data show more pairs of particles at small angles to each other and at angles near 180^o to each other than the phase-space model predicts. The distributions agree well with the jet model.

Figure 15 shows the observed single-particle inclusive x distribution for $E_{c.m.}$ = 7.4 GeV. The jet model reproduces this distribution quite well, but the the phase-space model predicts too few particles with x $\gtrsim$ 0.4. The agreement of this distribution with the jet model might be taken as further corroboration

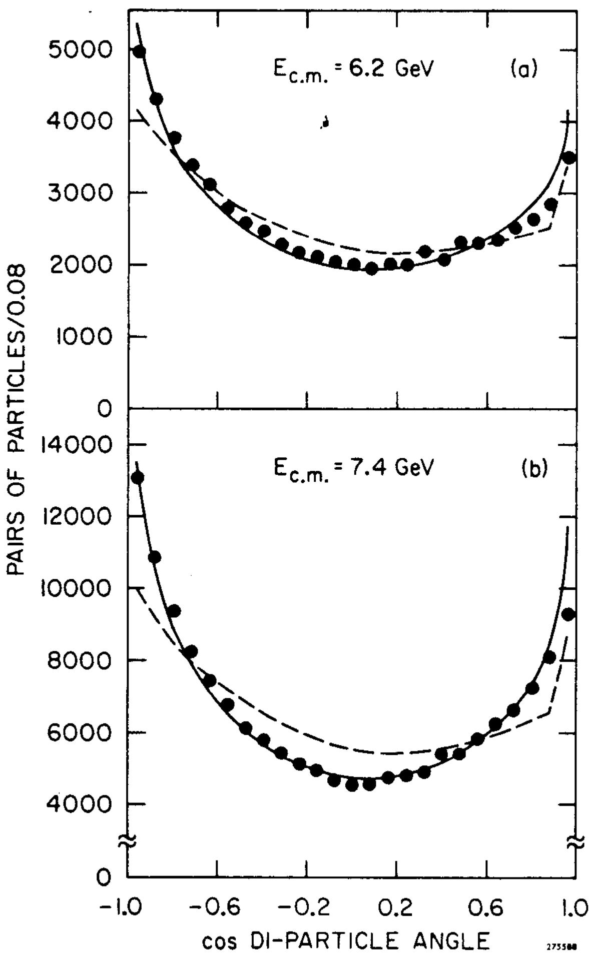

Fig. 14. Distributions of the cosine of diparticle angles for data, jet model (solid curves), and phase-space model (dashed curves) for (a) $E_{c.m.} = 6.2$ GeV and (b) $E_{c.m.} = 7.4$ GeV.

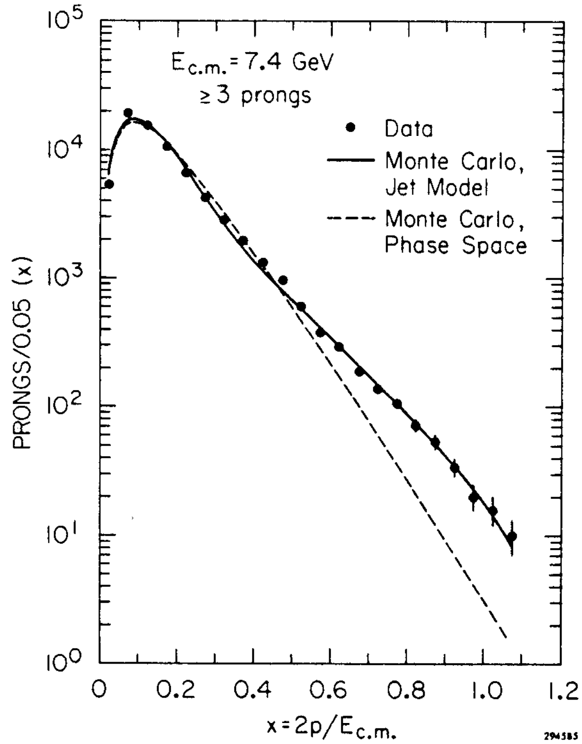

Fig. 15. Observed x distributions at $E_{c.m.} = 7.4$ GeV for data, jet model (solid curve), and phase-space model (dashed curve).

for the jet structure; however, events with a high-x particle tend to have low sphericity. It might be that the agreement of the S distributions with the jet model is due to the fact that the jet model produces a large enough number of high momentum particles. To determine whether the agreement of the S distributions is simply a consequence of the agreement of the x distributions, we examined the S distributions for those events in which no particle has $x > 0.4$. For these events the x distributions for both models agree with the data. The S distributions for such events at $E_{c.m.} = 7.4$ GeV are shown in Fig. 16(a). The jet model is still preferred over the phase-space model. The S distributions for events having a particle with $x > 0.4$ are shown in Fig. 16(b).

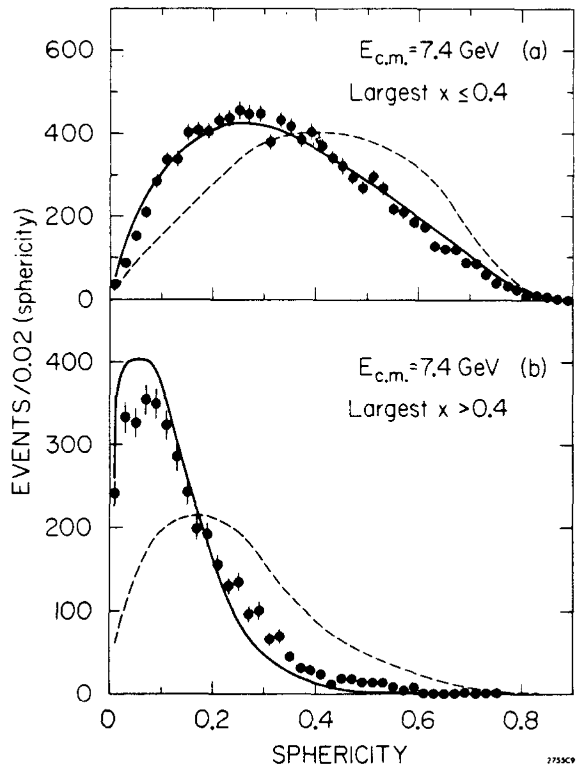

Fig. 16. Observed sphericity distributions at $E_{c.m.} = 7.4$ GeV for data, jet model (solid curves), and phase-space model (dashed curves) for (a) events with largest $x \leq 0.4$ and (b) events with largest $x > 0.4$.

Although the agreement is not perfect, the data are definitely in better agreement with the jet model. We therefore conclude that the agreement of the S distributions with the jet model is not due simply to the agreement of the x distributions and, furthermore, the agreement of the x distributions is a consequence of the jet structure. In fact, in the jet model the production of high-x particles is directly related to the limiting of transverse momentum relative to the jet axis.

Another possible cause for the appearance of jet structure is the production of resonances or new particles. Jet structure begins to be differentiated from phase space for energies above about 5 GeV. For these energies R is approximately constant and no structure has been seen. In order to search for jets which are actually the decays of particles or resonances we have plotted the distributions of observed masses of the jets as shown in Fig. 17 for $E_{c.m.} = 7.4$ GeV. The jet mass is the effective mass of all particles in an event on one side of a plane through the interaction vertex and perpendicular to the jet axis. Pion masses are used for all particles. Figure 17(a) shows the mass distribution for all jets. The spikes at masses of zero and the pion mass are due to zero-particle and one-particle jets, respectively. Most jet masses are less than 2 GeV/c^2. Figure 17(b) shows the mass distribution for 2-prong, charge-0 jets. We see that some jets are K_S^0's and that there is a shoulder at the ρ^0 mass. There is no evidence for the f^0. There is no evidence for structure in the mass distribution for 3-prong, charge-±1 jets, shown in Fig. 17(c). We conclude that there is no evidence for copious production of resonances which could lead to jet structure for most events. However, neutral particles are not detected and are therefore not included in the mass calculations. We have also not determined the effect of possible charmed particle production.

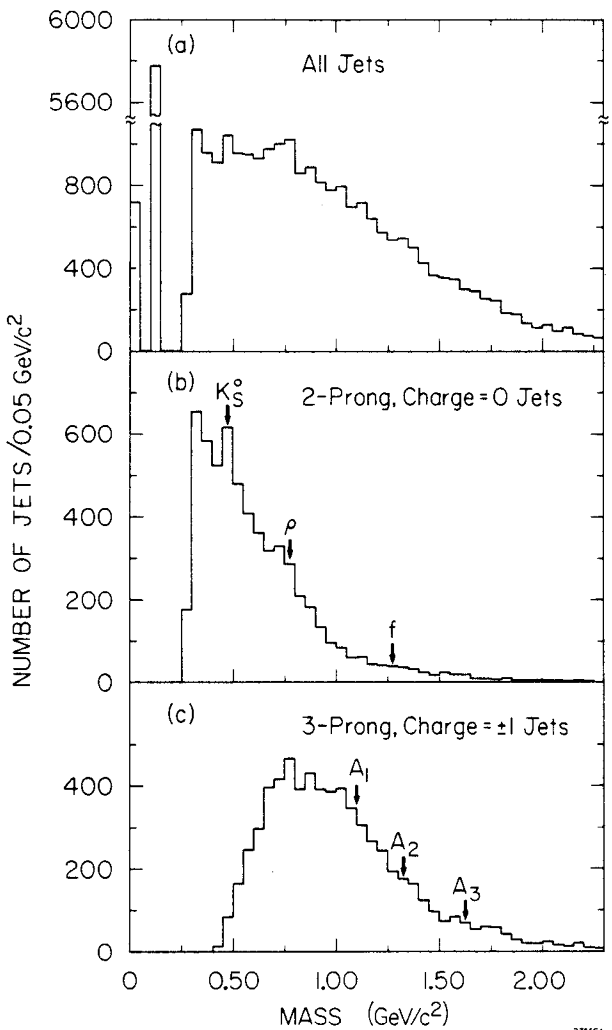

Fig. 17. Observed jet mass distributions at $E_{c.m.} = 7.4$ GeV for (a) all jets, (b) 2-prong, charge = 0 jets, and (c) 3-prong, charge = ±1 jets. Pion masses were used for all particles. The arrows indicate the masses of particles or resonances having the indicated decay modes.

The agreement of the observed sphericity distributions with the predictions of the jet model as opposed to phase space is evidence for jet structure in hadron production by e^+e^- annihilation.[20] A sample 7.4 GeV event, which illustrates the reconstructed jet axis and may illustrate a typical jet-like event, is shown in Fig. 18. This event has eight prongs, two of which have $x > 0.3$. The other six prongs have low momenta. The event has $S = 0.081$. The observed energy is less than $E_{c.m.}$ and the momenta do not balance, so there are missing particles.

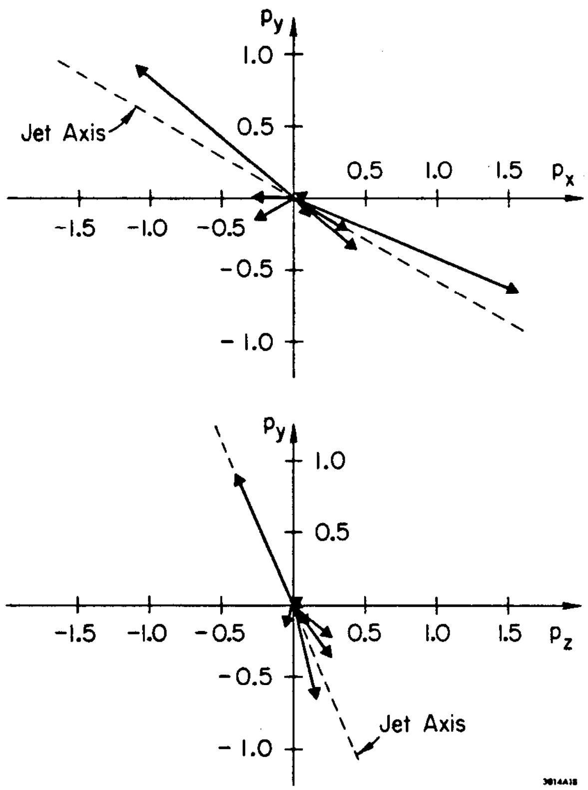

Fig. 18. Momentum space representation of a sample 7.4 GeV event. p_x, p_y, and p_z refer to the three spatial components of the particle momenta. The z-axis lies along the positron direction. This event has 8 prongs, 2 with $x > 0.3$. The reconstructed jet axis is represented by the dashed line. The event has $S = 0.081$.

V. JET AXIS AND INCLUSIVE ANGULAR DISTRIBUTIONS

The angular distributions of the hadrons and of the jet axis at 7.4 GeV will be presented in this section. At $E_{c.m.} = 7.4$ GeV the electron and positron beams at SPEAR are transversely polarized due to synchrotron radiation. The most general angular distribution for production through a single virtual photon is[21]

$$\frac{d\sigma}{d\Omega} \propto 1 + \alpha \cos^2\theta + P^2\alpha \sin^2\theta \cos 2\phi \ , \qquad (6)$$

where θ is the polar angle with respect to the incident e^+ direction, ϕ is the azimuthal angle with respect to the plane of the storage ring, P is the transverse polarization of each beam, and α is given by

$$\alpha = \frac{\sigma_T - \sigma_L}{\sigma_T + \sigma_L} \quad , \qquad (7)$$

where σ_T and σ_L are the transverse (helicity ± 1 along the particle direction) and longitudinal (helicity 0 along the particle direction) production cross sections. The transverse beam polarization allows us to measure α from the ϕ distribution which is quite useful because the magnetic detector has a small range of acceptance in $\cos^2\theta$ but full acceptance in ϕ.

For the QED reaction $e^+e^- \rightarrow \mu^+\mu^-$ the angular distribution is given by Eq. (6) with α=1. At $E_{c.m.} = 7.4$ GeV the muon pair data taken simultaneously with the hadronic data were used to determine an average value of $P^2 = 0.47 \pm 0.05$. Figure 19 shows the inclusive hadron ϕ distributions for particles with $x > 0.3$ and $|\cos\theta| \leq 0.6$ for $E_{c.m.} = 7.4$ GeV and $E_{c.m.} = 6.2$ GeV. At 7.4 GeV a strong

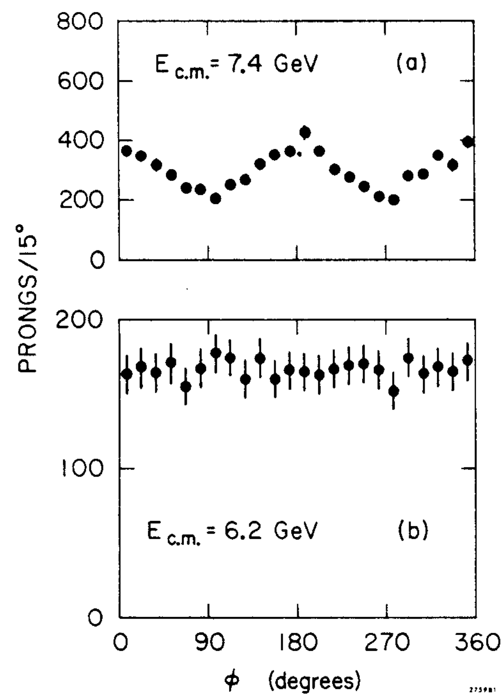

Fig. 19. Distributions of hadron prongs in azimuthal angle ϕ for prongs with $x > 0.3$ and $|\cos\theta| \leq 0.6$ for (a) $E_{c.m.} = 7.4$ GeV and (b) $E_{c.m.} = 6.2$ GeV.

inclusive hadron ϕ asymmetry is observed, while at 6.2 GeV, where the beams are unpolarized, the ϕ distribution is flat. The 6.2 GeV data was used to determine that the magnetic detector does not introduce a ϕ asymmetry. At 7.4 GeV the measured value of P^2 and the cos θ and ϕ distributions of the particles as a function of x were used to determine the inclusive hadron α as a function of x.[22] It was found that α is ≥ 0 and that α increases with increasing x. (The dependence of inclusive α on x at $E_{c.m.}$ = 7.4 GeV is shown in Fig. 21 along with a comparison with the Monte Carlo prediction.)

At 7.4 GeV a ϕ asymmetry was also observed for the jet axis. The ϕ distributions of the jet axis for jet axes with $|\cos\theta| \leq 0.6$ are shown in Fig. 20 for 6.2 and 7.4 GeV. (Since the jet axis is a symmetry axis, the angle $\phi + 180^{\circ}$ is equivalent to the angle ϕ.) At 6.2 GeV the beams are unpolarized and the ϕ distribution is flat, as expected. At 7.4 GeV the ϕ distribution of the jet axis shows an asymmetry with maxima and minima at the same values of ϕ as for $e^+e^- \to \mu^+\mu^-$.

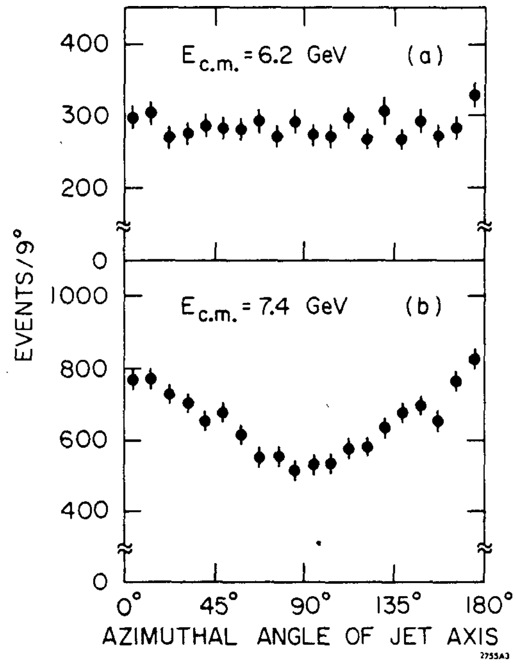

Fig. 20. Observed distributions of jet axis azimuthal angles from the plane of the storage ring for jet axes with $|\cos\theta| \leq 0.6$ for (a) $E_{c.m.}$ = 6.2 GeV and (b) $E_{c.m.}$ = 7.4 GeV.

The observed jet axis ϕ distribution and the measured value of P^2 were used to determine the parameter α for the jet axis angular distribution given by Eq. (6). The observed value of α for the jet axis was $\alpha = 0.50 \pm 0.07$. From the jet model Monte Carlo simulation, which included the angular distribution for the produced jet axis as given in Eq. (6), we found that the observed value of α will be less than the true value of α which describes the production of the jets because of the incomplete acceptance of the detector, the loss of neutral particles, and our method of reconstructing the jet axis. The simulation was used to calculate a ratio of observed to produced values of α of 0.52 at 7.4 GeV. This ratio was used to correct the observed α to obtain $\alpha = 0.97 \pm 0.14$ for the produced jet axis angular distribution. In terms of σ_L and σ_T this value of α corresponds to $\sigma_L/\sigma_T = 0.02 \pm 0.07$. The error in α is statistical only; we estimate that the systematic errors in the observed α can be neglected. However, there may be a systematic error in the correction factor relating the observed to the produced values of α due to model dependence.

The jet model can be used to predict the single particle inclusive angular distributions for all values of secondary particle momenta. In Fig. 21 values for the inclusive hadron α as a function of x at $E_{c.m.} = 7.4$ GeV are compared with the jet model calculation. The model assumed the value $\alpha = 0.97 \pm 0.14$ for the jet axis angular distribution. The prediction agrees well with the data for all values of x.

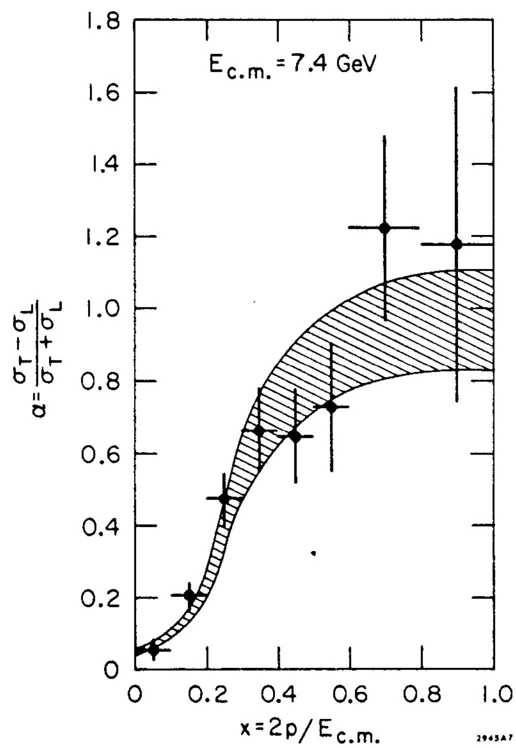

Fig. 21. Observed inclusive α vs. x for particles with $|\cos\theta| \leq 0.6$ in hadronic events at $E_{c.m.} = 7.4$ GeV. The prediction of the jet model Monte Carlo simulation for a jet axis angular distribution with $\alpha = 0.97 \pm 0.14$ is represented by the shaded band.

At energies other than 7.4 GeV it is not possible to determine the jet axis angular distribution with any accuracy because of the small beam polarization and subsequent absence of ϕ symmetry. The $\cos\theta$ distribution of the jet axis is too strongly affected by the small acceptance of the detector in $\cos\theta$. We are able, however, to measure the inclusive α versus x by fitting the inclusive $\cos\theta$ distributions. These determinations are less precise than those using polarized beams. Figure 22 shows preliminary values of inclusive hadron α versus x at $E_{c.m.} = 3.0$, 3.8, 4.1, 4.8,

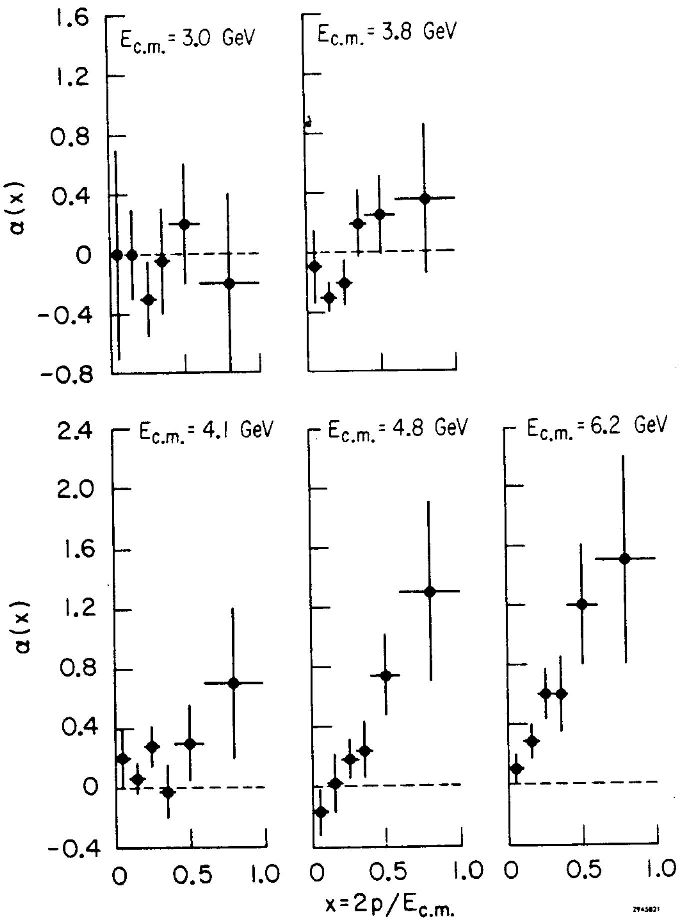

Fig. 22. Preliminary values for inclusive α vs. x obtained from fits of $1+\alpha(x)\cos^2\theta$ for $|\cos\theta| \leq 0.6$ for $E_{c.m.}$ = 3.0, 3.8, 4.1, 4.8, and 6.2 GeV.

and 6.2 GeV. At 3.0 GeV the inclusive α distribution is consistent with isotropy for all values of x. At 3.8 and 4.1 GeV there is some evidence for a $\cos^2\theta$ dependence at the larger values of x. At 4.8 and 6.2 GeV α definitely increases with increasing x and is, in fact, consistent with its maximum value of 1 at the higher values of x. The jet model simulation with a jet axis angular distribution of $1+\cos^2\theta$ can reproduce this dependence of α on x and $E_{c.m.}$ including the isotropy at 3.0 GeV. In fact, we begin to observe nonzero values for α just at energies where jet structure begins to be differentiated from phase space.

The data strongly support a jet hypothesis for hadron production in e^+e^- annihilation. The jet model Monte Carlo simulation reproduces not only the sphericity distributions for whole events but also the single particle inclusive momentum and angular distributions. The jet axis angular distribution integrated over azimuthal angle is proportional to $1+(0.97\pm0.14)\cos^2\theta$ at 7.4 GeV, giving $\sigma_L/\sigma_T = 0.02\pm0.07$. The jets are therefore produced with helicity ±1 along the jet axis. The jet axis angular distribution is consistent with that for a pair of spin-1/2 particles. In the framework of the quark-parton model, the partons must have spin-1/2 rather than spin 0.

VI. INCLUSIVE DISTRIBUTIONS IN VARIABLES RELATIVE TO THE JET AXIS

The limiting of transverse momentum relative to an axis for e^+e^- hadron production suggests a similarity with hadron-hadron interactions. In addition, if the jet structure is related to quark-partons, then one should examine the components of particle momenta relative to the parton direction, which is expected to be the jet axis, as is done in leptoproduction relative to the virtual photon direction. The inclusive hadronic cross section might be expected to be factorizable into a function of momentum parallel to the jet axis and a function of momentum perpendicular to that axis.

In order to investigate such questions, we have made a preliminary attempt to measure inclusive distributions of the hadrons in variables relative to the jet axis. For each hadronic event we reconstruct a jet axis as described in Section IV and calculate the components of each particle momentum parallel to ($p_\parallel$) and perpendicular to ($p_\perp$) the jet axis, as shown in Fig. 23.

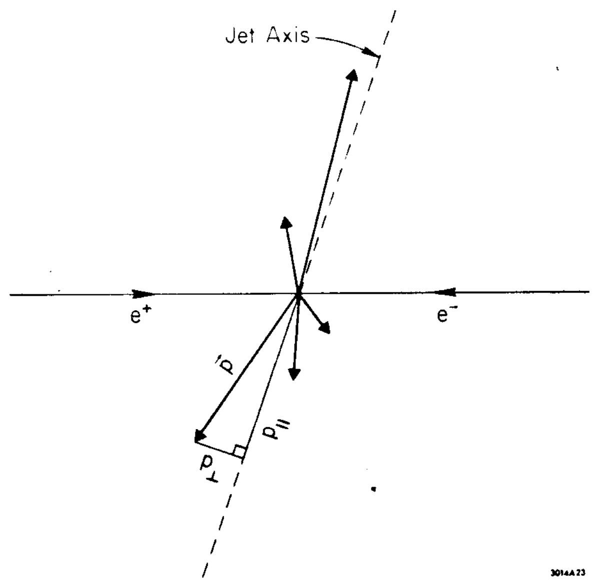

Fig. 23. Illustration of a hadronic event from e^+e^- annihilation showing the jet axis and the components of the momentum of a particle $\vec{p}$ parallel to ($p_\parallel$) and perpendicular to ($p_\perp$) the jet axis.

Since the inclusive quantity $s\,d\sigma/dx$, which was shown in Fig. 7, nearly scales, we are led to examine the inclusive distributions for $s\,d\sigma/dx_\parallel$, where $x_\parallel$, or Feynman x, is defined by

$$x_\parallel = 2p_\parallel/E_{c.m.} \quad , \tag{8}$$

shown in Fig. 24. These distributions have been corrected for geometric acceptance, trigger bias, and the method of reconstructing the jet axis by using the jet model Monte Carlo simulation. (The Monte Carlo corrections used to produce Fig. 7 were calculated using the same jet model Monte Carlo simulation as was used for Fig. 24 in order to eliminate systematic differences in the corrections due to different models.) Figure 25 shows the observed (before Monte Carlo

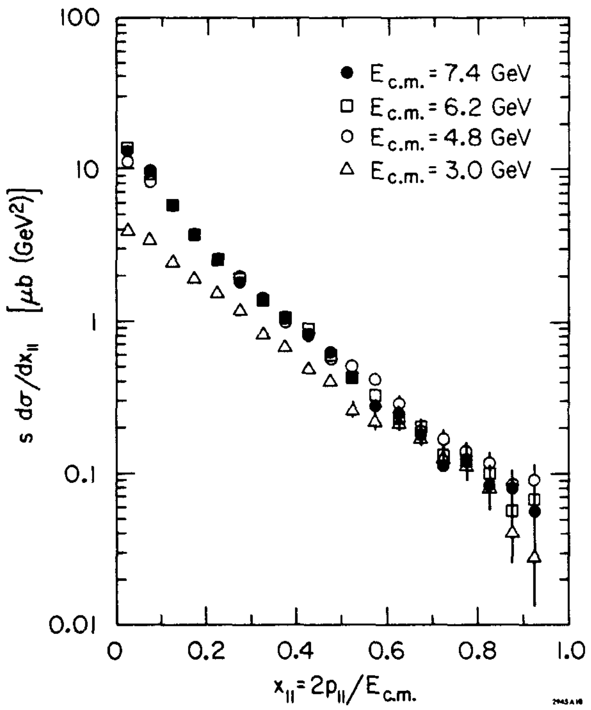

Fig. 24. $s\,d\sigma/dx_{\parallel}$ vs. $x_{\parallel}$ for $E_{c.m.}$ = 3.0, 4.8, 6.2, and 7.4 GeV. $x_{\parallel} = 2p_{\parallel}/E_{c.m.}$ where $p_{\parallel}$ is the component of particle momentum parallel to the jet axis.

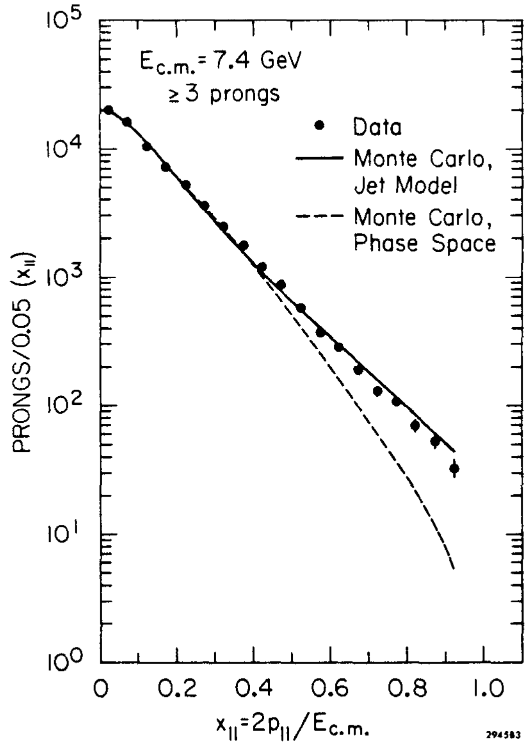

Fig. 25. Observed $x_{\parallel}$ distributions at $E_{c.m.}$ = 7.4 GeV for data, jet model (solid curve), and phase-space model (dashed curve).

corrections) inclusive $x_{\parallel}$ distribution for hadronic events with three or more prongs at $E_{c.m.}$ = 7.4 GeV compared with the predictions of the two models. As was the case for the x distribution, the jet model represents the data well and the phase-space model produces too few particles at large $x_{\parallel}$. By comparing Figs. 24 and 25 one can see that the Monte Carlo corrections do not make a large change in the shape of the $x_{\parallel}$ distribution. Corrections due to finding the wrong jet axis are not large for the $x_{\parallel}$ distribution mainly because the worst cases occur for events with only low momentum particles which are nearly isotropic.

If we compare the distributions in $s\,d\sigma/dx_{\parallel}$ with those in $s\,d\sigma/dx$, we see that as $E_{c.m.}$ increases the two distributions become more alike, presumably because

$p_\perp$ is a decreasing fraction of p. At the lowest energy $E_{c.m.} = 3.0$ GeV the two distributions are quite different. When e^+e^- inclusive momentum distributions are compared with those from hadron interactions or leptoproduction, they should be compared in terms of the variable $x_\parallel$. Unfortunately, we have not yet carried out such comparisons with other data. The $s\,d\sigma/dx_\parallel$ distributions are consistent with scaling for $x_\parallel \gtrsim 0.5$ for the entire energy range from 3.0 to 7.4 GeV. The 3.0 GeV distribution has a change in slope for $x_\parallel$ between 0.5 and 0.6. For $x_\parallel < 0.5$ the 3.0 GeV distribution has roughly the same slope as at the higher energies but is smaller in magnitude. From 4.8 to 7.4 GeV the $s\,d\sigma/dx_\parallel$ distributions are consistent with scaling over nearly the entire $x_\parallel$ range except for $x_\parallel < 0.1$.

The inclusive distributions in $p_\perp$ and rapidity are quite difficult to correct for the effects of finding the wrong jet axis. From Monte Carlo studies we have found that, unlike the $x_\parallel$ distribution, the produced and observed distributions are quite different if we use all events. For example, the jet model reproduces the observed $p_\perp$ distribution rather well when fitted to the mean $p_\perp$, as was shown in Fig. 10. However, the observed mean $p_\perp$ at 7.4 GeV was about 250 MeV/c whereas the produced mean $p_\perp$ was about 350 MeV/c. If we restrict ourselves to events which have a particle with $x > 0.5$, we can find the jet axis with some confidence and can use the Monte Carlo simulation to calculate corrections. (We could actually use the highest momentum particle as the jet axis in this case, but the reconstructed jet axis is closer to the true jet axis.) Therefore, for all of the remaining inclusive distributions we use only events which have a particle with $x > 0.5$ and we do not plot the highest-x particle (x_{max}) in the inclusive distribution. Distributions for the highest-x particle can be looked at separately but will not be presented here. The inclusive distributions are normalized to the total corss sections for events with a particle with $x > 0.5$ and are thus distributions of particle density in the variables used.

For comparison with the previous distributions we present distributions in $(1/\sigma)\, d\sigma/dx$, shown in Fig. 26, and $(1/\sigma)\, d\sigma/dx_{\parallel}$, shown in Fig. 27, for events with

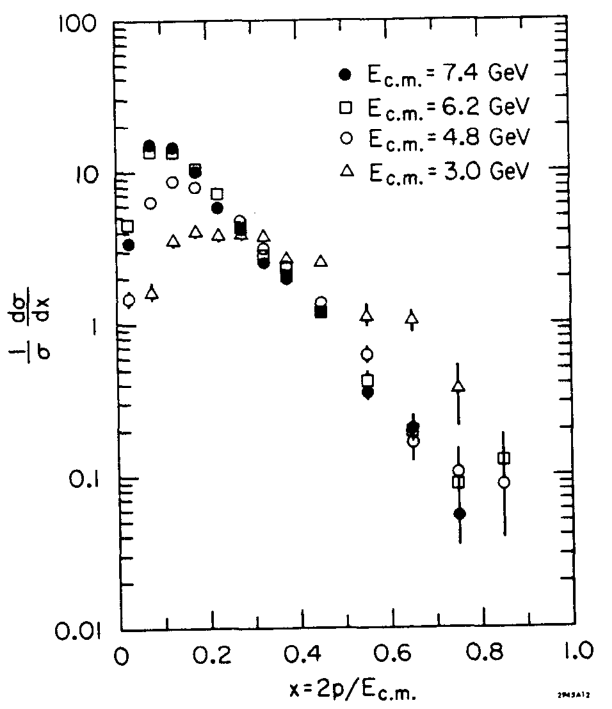

Fig. 26. $(1/\sigma)\, d\sigma/dx$ vs. x for events with x_{max} (the value of x for the highest-x particle) > 0.5 for $E_{c.m.}$ = 3.0, 4.8, 6.2, and 7.4 GeV. x_{max} is not plotted. The distributions are normalized to the cross sections for events with $x_{max} > 0.5$.

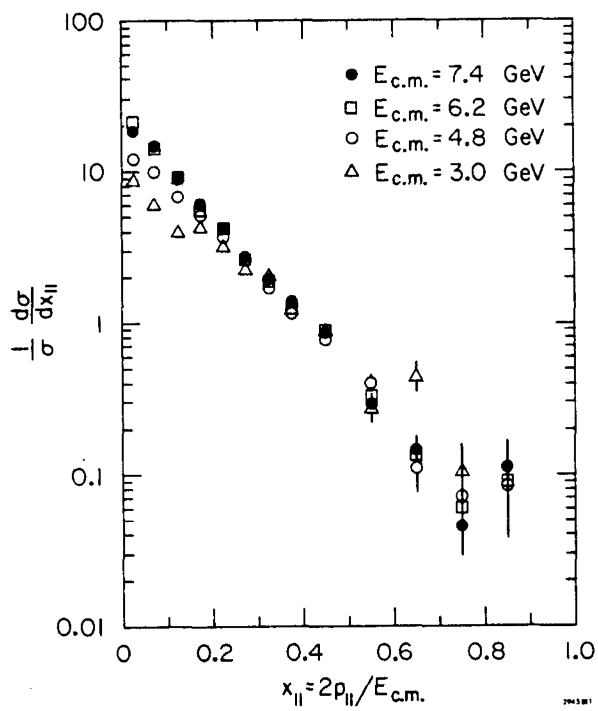

Fig. 27. $(1/\sigma)d\sigma/dx_{\parallel}$ vs. $x_{\parallel}$ for events with $x_{max} > 0.5$ for $E_{c.m.}$ = 3.0, 4.8, 6.2, and 7.4 GeV. x_{max} is not plotted. The distributions are normalized to the cross sections for events with $x_{max} >$ 0.5. $x_{\parallel} = 2p_{\parallel}/E_{c.m.}$ where $p_{\parallel}$ is the component of particle momentum parallel to the jet axis.

$x_{max} > 0.5$. The inclusive $(1/\sigma)\, d\sigma/dx$ distributions are similar in shape to the $s\, d\sigma/dx$ distributions for all events except that they have a steeper slope for large x for $E_{c.m.} \geq 4.8$ GeV. The data scale for $x \gtrsim 0.2$ for $E_{c.m.} \geq 4.8$ GeV as did the distributions for all events. The 3.0 GeV data do not scale, even at large x. The $(1/\sigma)\, d\sigma/dx_{\parallel}$ distributions also fall off more quickly for large $x_{\parallel}$ than do the $s\, d\sigma/dx_{\parallel}$ distributions for all events; for $x_{\parallel}$ this statement also applies to the 3.0 GeV data. The data also appear to scale for the entire energy range 3.0 to 7.4 GeV for $x_{\parallel} \gtrsim 0.2$, except for one 3.0 GeV point at $0.6 \leq x_{\parallel} < 0.7$. The change in slope for the 3.0 GeV data has moved to $x_{\parallel}$ between 0.1 and 0.2. Of course, we are now looking at "old" physics since "new" physics (i.e., charm) appears only in events with $x_{max} \lesssim 0.5$.

Figure 28 shows $(1/\sigma)\, d\sigma/dp_{\perp}$ versus $p_{\perp}$ for events with $x_{max} > 0.5$ for $E_{c.m.} = 3.0$, 4.8, 6.2, and 7.4 GeV. The highest-x particle is not included in the plots. We see that as $E_{c.m.}$ increases the shape of the distribution remains approximately the same. The area under the curves increases as $E_{c.m.}$ increases because of the increasing multiplicity. We have not determined the functional dependence of these distributions; the means of the distributions are about the same for the entire range of energies. It would certainly be interesting to be able to plot this distribution for all particles in all events; however, we do not know at this point how to correct the distributions for incorrect jet axis determinations for events with no high-momentum particles.

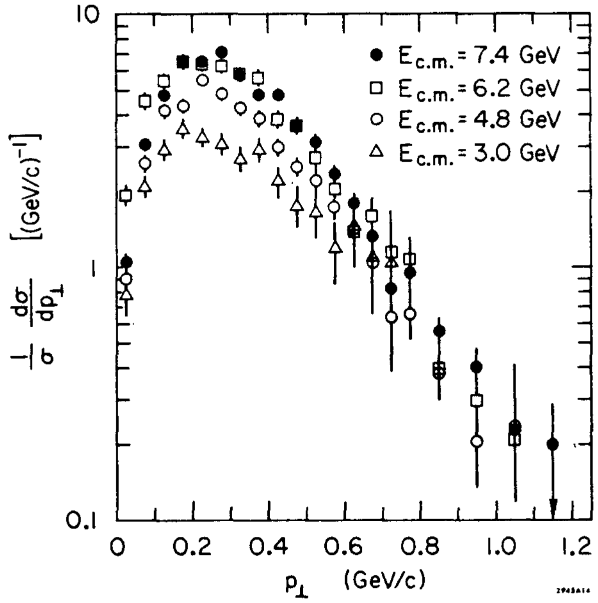

Fig. 28. $(1/\sigma)\, d\sigma/dp_{\perp}$ vs. $p_{\perp}$ for events with $x_{max} > 0.5$ for $E_{c.m.} = 3.0$, 4.8, 6.2, and 7.4 GeV. x_{max} is not plotted. The distributions are normalized to the cross sections for events with $x_{max} > 0.5$. $p_{\perp}$ is the component of particle momentum perpendicular to the jet axis.

In Fig. 29 we present distributions in rapidity with respect to the jet axis for events with $x_{max} > 0.5$ for $E_{c.m.} = 3.0$, 4.8, and 7.4 GeV. The rapidity is defined by

$$y = \frac{1}{2} \ln\left(\frac{E + p_{\parallel}}{E - p_{\parallel}}\right) , \tag{9}$$

where E is the energy of the particle with a pion mass assumed and $p_{\parallel}$ is the component of particle momentum parallel to the jet axis. The distributions are plotted in terms of $(1/\sigma)\, d\sigma/dy$. The widths of the distributions increase logarithmically

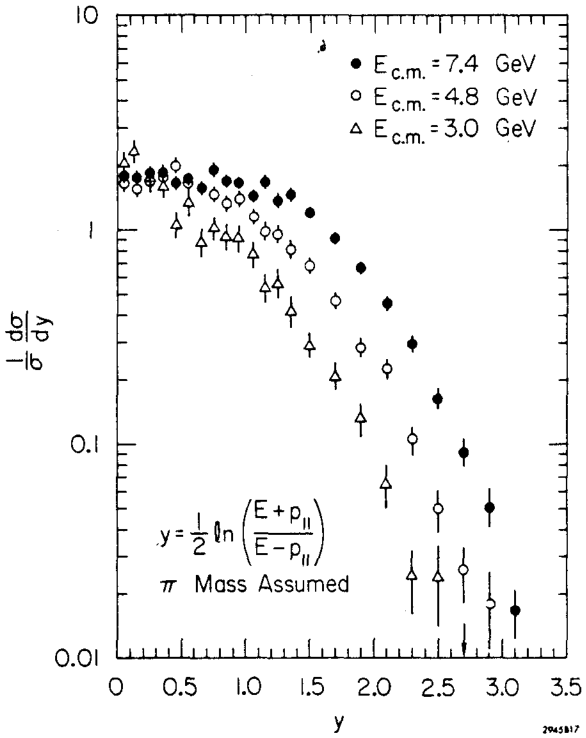

Fig. 29. $(1/\sigma)\, d\sigma/dy$ vs. y for events with $x_{max} > 0.5$ for $E_{c.m.} = 3.0$, 4.8, and 7.4 GeV. x_{max} is not plotted. The distributions are normalized to the cross sections for events with $x_{max} > 0.5$. y is the rapidity of the particle with respect to the jet axis. Pion masses were assumed.

with the energy. The magnitudes of the quantity $(1/\sigma)\, d\sigma/dy$ at $y \approx 0$ are approximately the same for each of the three energies. However, the distributions are normalized to the cross sections for events with $x_{max} > 0.5$. We do not know whether this sort of scaling is true for all events. At 7.4 GeV the rapidity distribution appears to develop a plateau.

Figure 30 shows a comparison between the rapidity distributions relative to the jet axis for e^+e^- and the rapidity relative to the beam direction for $pp \to \pi^+X$ and $pp \to \pi^-X$. The pp data were taken from Ref. 23. The data are plotted in terms of y_{lab} for the pp system. For pp the quantity plotted is $Ed^3\sigma/d^3p$, whereas for e^+e^- we plot $(1/\sigma)\, d\sigma/dy$. We intend to show only a qualitative comparison of shapes, not a quantitative comparison of magnitudes. The invariant cross sections are, of course, very different in magnitude and $(1/\sigma)\, d\sigma/dy$ for pp data was not available. Also, the pp data are plotted for $p_{\perp} = 0.4$ GeV/c, whereas the e^+e^- data is integrated over $p_{\perp}$. A comparison with Fermi Lab pp data[24] integrated over $p_{\perp}$ is, however, essentially the same. Since in pp interactions the protons take part of the energy which is then not available to pions, we have plotted the e^+e^- data in terms of y_{lab} for a pp system at a center-of-mass energy higher by two proton masses than for the e^+e^-

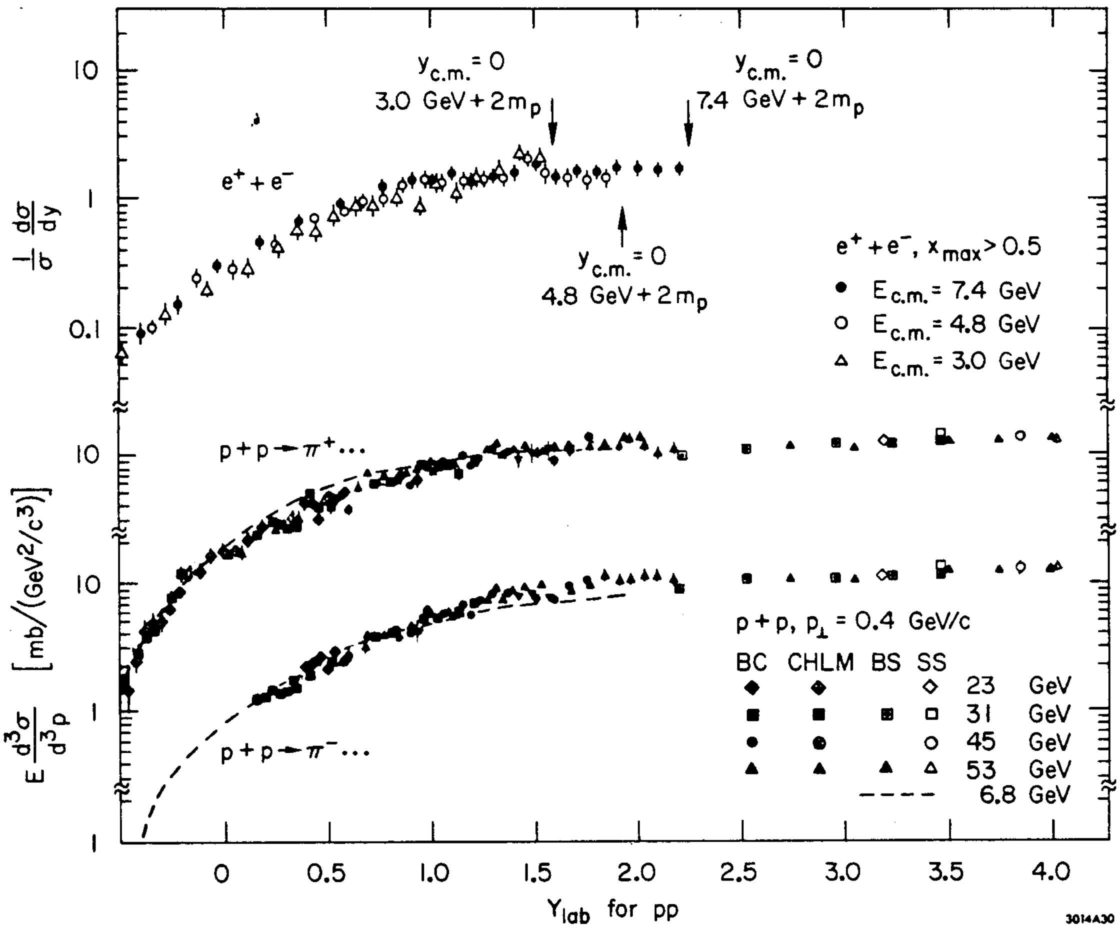

Fig. 30. Comparison of rapidity distributions in y_{lab} for e^+e^- and pp $\rightarrow \pi^+X$ or pp $\rightarrow \pi^-X$. The pp data were taken from Ref. 23. The e^+e^- data are those shown in Fig. 29 plotted in terms of y_{lab} for a pp system at a center-of-mass energy higher by 2 proton masses (m_p) than for the e^+e^- system.

system. We then see that the e^+e^- y_{lab} distributions have about the same shape as those for pp $\rightarrow \pi^+X$. The plateau begins to appear at about the same value of y_{lab} for both the e^+e^- and pp $\rightarrow \pi^+X$ data. If we compare the e^+e^- rapidity distribution with pp $\rightarrow \pi^-X$ in terms of y_{lab} for a pp system at a center-of-mass energy higher by about four proton masses than for the e^+e^- system, the shapes of the e^+e^- and pp $\rightarrow \pi^-X$ rapidity distributions are quite similar. Of course, for e^+e^- the π^+ and π^- rapidity distributions are the same and both charges of particles are plotted together.

VII. CONCLUSIONS

The data from hadron production by e^+e^- annihilation discussed here were taken by the SLAC/LBL magnetic detector collaboration at SPEAR at energies away from the resonances.

1. In the $E_{c.m.}$ range from 2.4 to 7.8 GeV, R shows the following behavior: below 3.5 GeV, R is approximately constant at a value of 2.5; between 3.5 and 4.8 GeV, R shows structure which may indicate the opening up of new channels; above 4.8 GeV, R is approximately constant again at a value of about 5.5.

2. There is strong evidence for jet structure in hadronic events at energies above about 5 GeV as shown by the agreement of the observed sphericity distributions with the jet model rather than the phase-space model predictions.

3. At $E_{c.m.} = 7.4$ GeV the jet axis angular distribution has been found to be proportional to $1+(0.97 \pm 0.14) \cos^2\theta$, giving $\sigma_L/\sigma_T = 0.02 \pm 0.07$. The jet axis angular distribution is consistent with that for a pair of spin-1/2 particles.

4. The quantity $s\, d\sigma/dx_{\parallel}$, where $x_{\parallel}$ (Feynman x) $= 2p_{\parallel}/E_{c.m.}$ and $p_{\parallel}$ is the component of particle momentum parallel to the jet axis, approximately scales for the $E_{c.m.}$ range 4.8 to 7.4 GeV.

5. The distributions in $p_{\perp}$ with respect to the jet axis, measured for events with a particle with $x > 0.5$, indicate that $p_{\perp}$ is approximately constant as $E_{c.m.}$ increases.

6. Distributions in rapidity with respect to the jet axis, measured for events with a particle with $x > 0.5$, show the development of a plateau at $E_{c.m.} = 7.4$ GeV. In the rapidity variable the jet axis looks qualitatively like the beam direction in pp collisions.

The data seem to be in general agreement with quark-parton constituent models. In order to explain the step in R, the models need at least one new heavy quark. It should be interesting to see what effect the production of (possibly) charmed particles will have on the conclusions drawn from the multiparticle properties of the hadronic events.

REFERENCES

1. A. Litke *et al.*, Phys. Rev. Lett. **30**, 1189 (1973);
   G. Tarnopolsky *et al.*, Phys. Rev. Lett. **32**, 432 (1974).
2. J.-E. Augustin *et al.*, Phys. Rev. Lett. **34**, 764 (1975).
3. J.-E. Augustin *et al.*, Phys. Rev. Lett. **33**, 1406 (1974);
   J. J. Aubert *et al.*, Phys. Rev. Lett. **33**, 1404 (1974).
4. G. S. Abrams *et al.*, Phys. Rev. Lett. **33**, 1453 (1974).
5. G. J. Feldman *et al.*, Phys. Rev. Lett. **35**, 821 (1975).
6. W. Tanenbaum *et al.*, Phys. Rev. Lett. **35**, 1323 (1975);
   W. Braunschweig *et al.*, Phys. Lett. B **57**, 407 (1975).
7. J. S. Whitaker *et al.*, to be published;
   G. H. Trilling *et al.*, to be published.
8. M. L. Perl *et al.*, Phys. Rev. Lett. **35**, 1489 (1975).
9. G. Goldhaber *et al.*, Phys. Rev. Lett. **37**, 255 (1976).
10. I. Peruzzi *et al.*, submitted to Phys. Rev. Lett.
11. Members of the SLAC/LBL magnetic detector collaboration are: G. S. Abrams, M. S. Alam, A. M. Boyarski, M. Breidenbach, W. C. Carithers, W. Chinowsky, R. G. DeVoe, J. M. Dorfan, G. J. Feldman, G. E. Fischer, C. E. Friedberg, D. Fryberger, G. Goldhaber, G. Hanson, J. A. Jaros, A. D. Johnson, J. A. Kadyk, R. R. Larsen, D. Lüke, V. Lüth, H. L. Lynch, R. J. Madaras, C. C. Morehouse, H. K. Nguyen, J. M. Paterson, M. L. Perl, I. Peruzzi, M. Piccolo, F. M. Pierre, T. P. Pun, P. Rapidis, B. Richter, R. H. Schindler, R. F. Schwitters, J. Siegrist, W. Tanenbaum, G. H. Trilling, F. Vannucci, J. S. Whitaker, and J. E. Wiss. Previous members of the collaboration, who should also be given credit, are: J.-E. Augustin, D. Briggs, F. Bulos, J. T. Dakin, R. J. Hollebeek, B. Jean-Marie, D. Lyon, F. C. Winkelmann, and J. E. Zipse.
12. J.-E. Augustin *et al.*, Phys. Rev. Lett. **34**, 233 (1975).

13. Gary J. Feldman and Martin L. Perl, Physics Reports C 19, 233 (1975).

14. This is an important point because events in which a pair of heavy leptons are produced are expected to occur predominantly in the two-prong sample. See Y. S. Tsai, Phys. Rev. D 4, 2821 (1971) and K.J.F. Gaemers and R. Raitio, Stanford Linear Accelerator Center preprint SLAC-PUB-1727 (1976), submitted to Phys. Rev. D.

15. R. F. Schwitters in Proceedings of the International Symposium on Lepton and Photon Interactions at High Energies (Stanford University, Stanford, California, 1975); p. 5.

16. S. D. Drell, D. J. Levy, and T. M. Yan, Phys. Rev. 187, 2159 (1969), and Phys. Rev. D 1, 1617 (1970).

17. N. Cabibbo, G. Parisi, and M. Testa, Lett. Nuovo Cimento 4, 35 (1970).

18. J. D. Bjorken and S. J. Brodsky, Phys. Rev. D 1, 1416 (1970).

19. R. P. Feynman, Photon-Hadron Interactions (W. A. Benjamin, Inc., 1972); p. 166.

20. We have reported evidence for jet structure in hadron production by e^+e^- annihilation previously: Gail Hanson in Proceedings of the Summer Institute on Particle Physics, SLAC-191 (Stanford Linear Accelerator Center, Stanford University, Stanford, California, 1975); p. 237. G. Hanson et al., Phys. Rev. Lett. 35, 1609 (1975).

21. Yung Su Tsai, Phys. Rev. D 12, 3533 (1975).

22. R. F. Schwitters et al., Phys. Rev. Lett. 35, 1320 (1975).

23. P. Capiluppi et al., Nucl. Phys. B 79, 189 (1974).

24. T. Ferbel in Proceedings of the Summer Institute on Particle Physics, SLAC-179 (Stanford Linear Accelerator Center, Stanford University, Stanford, California, 1974); Vol. II, p. 175.